INTERNATIONAL JOURNAL FOR NUMERICAL METHODS IN FLUIDS
Int. J. Numer. Meth. Fluids 2001; **36**: 351–371 (DOI: 10.1002/fld.138)

Advection upwinding splitting method to solve a compressible two-fluid model

Yang-Yao Niu*,[1]

Institute of Mechanical and Aerospace Engineering, Chung-Hua University, Hsin-Chu, 30067 Taiwan, Republic of China

SUMMARY

In this study, the advection upwinding splitting method (AUSM) is modified for the resolution of two-phase mixtures with interfaces. The compressible two-fluid model proposed by Saurel and Abgrall is chosen as the model equations. Dense and dilute phases are described in terms of the volume fraction and equations of state to represent multi-phase mixtures. Test cases involving an air–water shock tube, water faucet, and dilute particulate turbulent flows through a 90° bend are used to verify the current work. It is shown that the AUSM based on flux differences (AUSMD) contains the mechanism to correctly capture the contact discontinuity and interfaces between phases. In addition, a successful application to dilute particulate turbulence flows by the AUSMD is demonstrated. Copyright © 2001 John Wiley & Sons, Ltd.

KEY WORDS: AUSMD; multi-phase flow; two-fluid model

1. INTRODUCTION

Currently, understanding compressible multi-phase flow phenomena by means of computational methodology is required in the safety analysis of chemical reactor utilities and engine combustion processes. As noted by Saurel and Abgrall [1,2], a compressible multi-phase flow is always regarded as a carrier phase containing a lot of individual particles, droplets, or bubbles, with interfaces in each control volume. Among phases, there are different physical or thermodynamic properties which are separated by interfaces. One common way of solving compressible multi-phase flow problems is usually based on the so-called two-fluid model, which considers the carrier phase and the disperse phase as interpenetrating continua coexisting at every point in space. In the two-fluid model, each phase is separately described

* Correspondence to: Department of Mechanical Engineering, Institute of Aeronautics and Astronautics, Chung-Hua University, 30 Tung Shiang, Hsin-Chu, 30067 Taiwan, Republic of China.
[1] E-mail: yniu@chu.edu.tw

Received November 1999
Revised March 2000

in terms of two sets of conservation equations, whereas the exchange of momentum and energy takes place across the interfaces. Therefore, an accurate resolution of flow physics near interfaces is essential to solve the compressible two-fluid model. Over the past years, the development to solve the two-fluid model has achieved a lot of progress by means of convection schemes [3–7] or Riemann solvers [8–11]. However, conservative Euler solvers have been found to produce numerical oscillations near interfaces. As explained in References [12–14], the averaging procedure in the conservative formulation causing numerical mixing often fails to maintain pressure equilibrium among fluid composition across material interfaces. It has also been found that updating the pressure field via the equation of state often generates erroneous pressure fluctuations at material interfaces, which subsequently contaminate the solution of other flow variables. In order to overcome numerical difficulties from the multi-fluid calculations, great efforts have been geared toward many directions. To our knowledge, Abgrall [15] uses a quasi-conservative formulation of the equations to ensure a consistent approximation of the energy equation near the interfaces, where regions of different fluid components are separated. Abgrall solves an additional transport equation for $1/(\gamma - 1)$ to update γ with other conservative equations based on the Roe approximated Riemann solver for mixtures of two perfect gases. To remove conservation errors around material fronts, Jenny *et al.* [14] modified the total energy per unit time in conservative Euler solvers to avoid the occurrence of the pressure errors generated near the interfaces. However, it is unclear how to extend the correction to deal with the real gas flows. Another approach introduced by Karni [13] is to solve the problem by employing a non-conservative primitive Euler formulation, which uses a small viscous perturbation technique to remove leading-order conservation errors. Also, Karni [16] solved multi-component fluids augmented by the pressure evolution equation derived from the energy equation that exhibits oscillation-free interfaces. This method is not exactly conservative at the interface; however, negligible relative conservation errors only in the total energy are obtained for the very strong shocks. Subsequently, Shyue [17] extended the work of Abgrall [12,15] from polytropic gases in one dimension to a stiffened gas with the so-called stiffened gas equation of state to approximate materials, including compressible liquids and solids. The system of equations is solved by using a high-resolution wave propagation method [18]. Shyue modified the Roe-type Riemann solver by assuming velocity and pressure equilibrium in each grid cell. It shows that monotone profiles of flow solutions near material front and pressure equilibrium are achieved. However, the reconstruction of the numerical flux is expressed in a sophisticated way. The derivation of the eigensystem requires tedious work for solving multi-dimensional complicated multi-flow problems. In our previous work [19], the two-phase model derived by Shyue [17] is modified in a conservation form and solved by the advection upwinding splitting method (AUSM) based on flux difference (AUSMD) [20,21]. Numerical results show that the AUSMD not only enhances pressure equilibrium across the interface but also keeps pressure continuous across the contact discontinuity between phases.

To continue this effort, the AUSMD is applied to solve a seven-equation compressible two-fluid model suggested by Saurel and Abgrall [1] here. In this model, a multi-phase flow is assumed as a multi-fluid flow with an extremely large number of interfaces, described by means of a non-conservative revolution equation of volume fraction. An accurate resolution of interfaces is required. Saurel and Abgrall have developed a successful Harten, Lax and van

Leer (HLL)-type Riemann solver to compute the model. However, the estimation of wave speed in HLL Riemann solver leaves many choices. In this study, the idea of the AUSMD [20] is introduced to solve the two-fluid model of Saurel and Abgrall in a simpler form. A non-conservative approach based on AUSM-type formulations is suggested to simulate the evolution of volume fraction to avoid numerical oscillations near material interfaces. In addition to solving the convective terms for the dense phase, a modification of the AUSM is also applied to compute the equations for the dilute phase. Besides, some compressible multi-phase flows are usually in the low-Mach number flow limit. Numerical convergence difficulties caused by wide disparities in eigenvalues are widely encountered in the calculations. Therefore, in this study the AUSMD incorporated with the eigenvalue rescaled techniques by Edwards and Liou [22] is chosen to circumvent the convergence difficulties for the low-speed multi-phase flow problems. In addition, the predictor–corrector approach suggested by Saurel and Abgrall [1] is used to discretize numerical time accuracy. Meanwhile, high-order spatial accuracy is obtained through the monotone upstream-centered scheme for the conservation laws (MUSCL) method with limiter functions [23]. In numerical verifications, an air–liquid shock tube [17], water faucet [24], and a dilute particulate turbulent flow through a 90° bend [25,26] are chosen. Grid refinement is also performed.

2. GOVERNING EQUATIONS

The two-fluid modeling strategy considers each phase separately in terms of an independent set of momentum, mass, and energy equations. The interactions between the two phases are described by the coupling of volume fraction and transfer terms of mass, momentum, and energy of each phase. This study solves a multi-dimensional, seven-equation, two-fluid model transport equations, which are proposed by Saurel and Abgrall [1]. It involves six equations obtained from conservation laws for carrier phase and disperse phase, and completed by a seventh equation for the revolution of the volume fraction as the followings:

Volume fraction equation

$$\frac{\partial}{\partial t}(\alpha_g) + (V_I)\frac{\partial}{\partial x_k}(\alpha_g) = 0 \tag{1a}$$

Mass conservation

$$\frac{\partial}{\partial t}(\alpha_g \rho_g) + \frac{\partial}{\partial x_k}(\alpha_g \rho_g u_{g,k}) = \dot{M}, \qquad \frac{\partial}{\partial t}(\alpha_p \rho_p) + \frac{\partial}{\partial x_k}(\alpha_p \rho_p u_{p,k}) = -\dot{M} \tag{1b}$$

Momentum conservation

$$\frac{\partial}{\partial t}(\alpha_g \rho_g u_{g,k}) + \frac{\partial}{\partial x_k}(\alpha_g \rho_g u_{g,k} u_{g,j} + \alpha_g P_g) = P_I \frac{\partial \alpha_g}{\partial x_k} + \dot{M} V_I + F_d$$

$$\frac{\partial}{\partial t}(\alpha_{\mathrm{p}}\rho_{\mathrm{p}}u_{\mathrm{p},k}) + \frac{\partial}{\partial x_k}(\alpha_{\mathrm{p}}\rho_{\mathrm{p}}u_{\mathrm{p},k}u_{\mathrm{p},j} + \alpha_{\mathrm{p}}P_{\mathrm{p}}) = -P_{\mathrm{I}}\frac{\partial \alpha_{\mathrm{g}}}{\partial x_k} - \dot{M}V_{\mathrm{I}} - F_{\mathrm{d}} \tag{1c}$$

Energy conservation

$$\frac{\partial}{\partial t}(\alpha_{\mathrm{g}}\rho_{\mathrm{g}}E_{\mathrm{g},k}) + \frac{\partial}{\partial x_k}u_{\mathrm{g},k}(\alpha_{\mathrm{g}}\rho_{\mathrm{g}}E_{\mathrm{g}} + \alpha_{\mathrm{g}}P_{\mathrm{g}}) = P_{\mathrm{I}}V_{\mathrm{I}}\frac{\partial \alpha_{\mathrm{g}}}{\partial x} + \dot{M}E_i + F_{\mathrm{d}}V_{\mathrm{I}} + Q_i$$

$$\frac{\partial}{\partial t}(\alpha_{\mathrm{g}}\rho_{\mathrm{g}}E_{\mathrm{p},k}) + \frac{\partial}{\partial x_k}u_{\mathrm{p},k}(\alpha_{\mathrm{p}}\rho_{\mathrm{p}}E_{\mathrm{p}} + \alpha_{\mathrm{g}}P_{\mathrm{p}}) = -P_{\mathrm{I}}V_{\mathrm{I}}\frac{\partial \alpha_{\mathrm{g}}}{\partial x} - \dot{M}E_i - F_{\mathrm{d}}V_{\mathrm{I}} - Q_i \tag{1d}$$

Energy compatibility

$$\alpha_{\mathrm{p}} + \alpha_{\mathrm{g}} = 1 \tag{1e}$$

In the above equations, α stands for the phase volume fraction and ρ, u, and E are density, velocity, and total energy for each phase respectively. The total energy $E_k = e_k + \frac{1}{2}u_k$, where e is denotes the internal energy. The subscripts 'g' and 'p' represent the carrier phase and disperse phase respectively. The interfacial variables have the subscript 'I'. The transfer terms of the right-hand sides of the same equations are mass transfer $\dot{M}$, drag force F_{d}, convective heat transfer Q_i, and the non-conservative terms

$$P_{\mathrm{I}}\frac{\partial \alpha_{\mathrm{g}}}{\partial x_k} \quad \text{and} \quad P_{\mathrm{I}}V_{\mathrm{I}}\frac{\partial \alpha_{\mathrm{g}}}{\partial x}$$

The above equations can be supplemented by two equations of state: $p_k = p_k(\rho_k, e_k)$.The pressure P_{I} and the velocity V_{I} represent the averaged values of the interfacial area over the two-phase control volume. The mean interfacial pressure defined in Reference [1] is considered equal to the mixture pressure, namely

$$P_{\mathrm{I}} = \alpha_{\mathrm{p}}P_{\mathrm{p}} + \alpha_{\mathrm{g}}P_{\mathrm{g}} \tag{2}$$

and the mean interfacial velocity is assumed to correspond to the center of the mass velocity, like

$$V_{\mathrm{I}} = \frac{\alpha_{\mathrm{p}}\rho_{\mathrm{p}}u + \alpha_{\mathrm{g}}\rho_{\mathrm{g}}u_{\mathrm{g}}}{\alpha_{\mathrm{p}}\rho_{\mathrm{p}} + \alpha_{\mathrm{g}}\rho_{\mathrm{g}}} \tag{3}$$

with the mixture density as

$$\rho = \alpha_{\mathrm{p}}\rho_{\mathrm{p}} + \alpha_{\mathrm{g}}\rho_{\mathrm{g}} \tag{4}$$

2.1. Dilute particulate turbulence models

In this paper, using the AUSMD to solve dilute particulate flow problems by means of the two-fluid model strategy is also discussed. Under the conditions of moderate or low pressures [1], compressibility effects of the particulate phase can be neglected. Following dilute particulate phase assumptions discussed in References [6,7] a dilute particulate turbulence flow model based on the renormalization group theory (RNG) proposed by Tu and Fletcher can be obtained as

$$\frac{\partial}{\partial t}(\alpha_{\mathrm{g}}\rho_{\mathrm{g}}u_{\mathrm{g},k}) + \frac{\partial}{\partial x_k}(\alpha_{\mathrm{g}}\rho_{\mathrm{g}}u_{\mathrm{g},k}u_{\mathrm{g},j}) = -\frac{\partial(\alpha_{\mathrm{g}}P)}{\partial x_k} + \frac{\partial}{\partial x_k}\left(\alpha_{\mathrm{g}}\rho_{\mathrm{g}}\nu_{\mathrm{gl}}\frac{\partial}{\partial x_j}u_{\mathrm{g},k}\right) - \frac{\partial}{\partial x_k}(\alpha_{\mathrm{g}}\rho_{\mathrm{g}}\overline{u_{\mathrm{g},k}u_{\mathrm{g},j}}) - F_{D,k} \tag{5}$$

$$\frac{\partial}{\partial t}(\alpha_{\mathrm{p}}\rho_{\mathrm{p}}u_{\mathrm{p},k}) + \frac{\partial}{\partial x_k}(\alpha_{\mathrm{p}}\rho_{\mathrm{p}}u_{\mathrm{p},k}u_{\mathrm{p},j}) = -\frac{\partial(\alpha_{\mathrm{p}}P)}{\partial x_k} + \frac{\partial}{\partial x_k}\left(\alpha_{\mathrm{p}}\rho_{\mathrm{p}}\nu_{\mathrm{pl}}\frac{\partial}{\partial x_j}u_{\mathrm{p},k}\right) - \frac{\partial}{\partial x_k}(\alpha_{\mathrm{p}}\rho_{\mathrm{p}}\overline{u_{\mathrm{p},k}u_{\mathrm{p},j}}) - F_{D,k} + \alpha_{\mathrm{p}}\rho_D G_k \tag{6}$$

where the source terms F_D due to the slip velocity of the two phases is defined by

$$F_{D,k} = \frac{\rho_{\mathrm{p}} f(u_{\mathrm{g},k} - u_{\mathrm{p},k})}{t_{\mathrm{p}}} \tag{7}$$

and the particle response time t_{p} is

$$t_{\mathrm{p}} = \frac{\rho_{\mathrm{s}} d_{\mathrm{p}}^2}{18\rho_{\mathrm{g}}\nu_{\mathrm{gl}}} \tag{8}$$

where ρ_{s} the material density of particles and the correction factor f is defined by

$$f = \begin{cases} 1 + 0.15Re_{\mathrm{p}}^{0.687} & 0 < Re_{\mathrm{p}} \le 200 \\ 0.914Re_{\mathrm{p}}^{0.282} + 0.0135Re_{\mathrm{p}} & 200 < Re_{\mathrm{p}} \le 2500 \\ 0.0167Re_{\mathrm{p}} & 2500 < Re_{\mathrm{p}} \end{cases} \tag{9}$$

with the particulate Reynolds number

$$Re_{\mathrm{P}} = \frac{|u_{\mathrm{g},k} - u_{\mathrm{p},k}|d_{\mathrm{p}}}{\nu_{\mathrm{g}}} \tag{10}$$

and d_{p} is the diameter of the particle. The second-order correlation terms for the particle phase using a gradient hypothesis [6] are

$$-\rho_p \alpha_p \overline{u'_p u'_{p,j}} = \mu_p \rho_p \alpha_p \left(\frac{\partial u_{p,i}}{\partial x_j} + \frac{\partial u_{p,j}}{\partial x_i} \right) \tag{11}$$

Besides, a RNG based $k-\varepsilon$ turbulence model suggested by Yakhot and Orszag [27] and modified by Tu and Fletcher [6,7] is employed. The kinetic energy of the turbulence k and its dissipation rate ε are governed by separate transport equations, such as

$$\frac{\partial}{\partial t}(\alpha_p \rho_g k) + \frac{\partial}{\partial x_k}(\alpha_p \rho_g u_{g,k} k) = \frac{\partial}{\partial x_k}\left(\alpha_p \rho_g \nu_{gt} \frac{\partial k}{\partial x_k} \right) + P - \alpha_p \rho_g \varepsilon + S_k$$

$$\frac{\partial}{\partial t}(\alpha_p \rho_g \varepsilon) + \frac{\partial}{\partial x_k}(\alpha_p \rho_g u_{g,k} \varepsilon) = \frac{\partial}{\partial x_k}\left(\alpha_g \rho_g \nu_{gt} \frac{\partial \varepsilon}{\partial x_k} \right) + \frac{\varepsilon}{k}(C_1 P - C_2 \alpha_p \rho_g \varepsilon) - \rho_g R + S_\varepsilon \tag{12}$$

In the RNG turbulence transport equation, an inverse Prandtl number α is introduced and can be obtained from the following equation:

$$\left| \frac{\alpha - 1.3929}{\alpha_0 - 1.3929} \right|^{0.6321} \left| \frac{\alpha + 2.3929}{\alpha_0 + 2.3929} \right|^{0.3679} = \frac{\nu_{gl}}{\nu_{eff}} \tag{13}$$

where $\alpha_0 = 1$ and ν_{gl} is the laminar viscosity of the gas phase and the turbulent viscosity $\nu_{gt} = \nu_{eff} - \nu_{gl}$ and the effective viscosity is given by

$$\nu_{eff} = \nu_l \left[1 + \sqrt{\frac{C_u}{\nu_l}} \frac{k}{\sqrt{\varepsilon}} \right]^2 \tag{14}$$

The extra source terms in Equation (12) contain the interaction between the particles and the gas phase for when the turbulence modulation of both phases is considered. The production of turbulent energy is based on Boussinesq's approximation, and is expressed as

$$P = -\rho \overline{u''_i u''_j} \frac{\partial u_i}{\partial x_j} = \left[\mu_{gt} \left(\frac{\partial u_j}{\partial x_i} + \frac{\partial u_i}{\partial x_j} - \frac{2}{3}(\nabla \cdot \vec{V}) \delta_{ij} \right) - \frac{2}{3} \rho k \delta_{ij} \right] \frac{\partial u_i}{\partial x_j} \tag{15}$$

and the rate of strain term R is given as

$$R = \frac{C_u \eta^3 (1 - \eta/\eta_0)}{1 + \kappa \eta^3} \frac{\varepsilon^2}{k} \tag{16}$$

where $C_u = 0.09$, $C_1 = 1.42$, $C_2 = 1.68$, $\eta = \sigma k/\varepsilon$, $\eta_0 = 4.38$, $\kappa = 0.012$, $\sigma = \sqrt{2 S_{ij} S_{ij}}$, and

$$S_{ij} = \frac{1}{2}\left(\frac{\partial u_i}{\partial x_j} + \frac{\partial u_j}{\partial x_i} \right)$$

Also the effects of particles on the gas turbulence formation [7] are modeled by

$$S_k = -2k\frac{\rho_p}{t_p}\left[1-\exp\left(-B_k\frac{t_p}{t_L}\right)\right] \tag{17}$$

and

$$S_\varepsilon = -2\varepsilon\frac{\rho_p}{t_p}\left[1-\exp\left(-B_\varepsilon\frac{t_p}{t_L}\right)\right] \tag{18}$$

where the particle response time is found in Equation (8); ρ_p is the bulk density of the particle phase, $B_K = 0.09$, $B_\varepsilon = 0.4$, and $t_L = k/\varepsilon$.

3. NUMERICAL METHOD

The system of equations (1a)–(1e) has been shown to be a strictly hyperbolic model in previous works. This allows us to apply existing hyperbolic solvers as approximate Riemann solvers or as a flux vector splitting method, which have successfully solved the single-phase problems, to simulate the current two-phase model. First, the system equations can be written in a compact form

$$\frac{\partial\alpha}{\partial t} + V_I\frac{\partial\alpha}{\partial x} = 0 \tag{19}$$

$$\frac{\partial U}{\partial t} + \frac{\partial F}{\partial x} = H(U)\frac{\partial\alpha_g}{\partial x} \tag{20}$$

where $U = (\alpha_k\rho_k, \alpha_k\rho_k u_k, \alpha_k\rho_k E_k)$, $F = [\alpha_k\rho_k u_k, \alpha_k\rho_k u_k^2 + \alpha_k P_k, u_k(\alpha_k\rho_k E_k + \alpha_k P_k)]$, and $H = (0, p_I + p_I v_I)$. It involves non-conservative terms coupling with six-equation conservation equations and a non-conservative evolution equation of void fraction. Numerical solutions of the system of equations (1a)–(1e) are evolved by a succession of operators [1] with a constant time step, as

$$U_i^{n+1} = L_s^{\Delta t} L_h^{\Delta t} U_i^n \tag{21}$$

where $L_h^{\Delta t}$ denotes the hyperbolic operator as

$$U_i^{n+1} = U_i^n - \frac{\Delta t}{\Delta x}(F_{i+1/2}^n - F_{i-1/2}^n) + \Delta t H(U_i^n)\frac{\alpha_{i+1}^n - \alpha_{i-1}^n}{2\Delta x} \tag{22}$$

and $L_s^{\Delta t}$ denotes the integration operator for source and relaxation terms seen in Reference [28]. The interface numerical flux, $F_{j+1/2} = F_{j+1/2,R} + F_{j+1/2,L}$, can be accomplished by the AUSMD. By means of the MUSCL method with a minmod limiter [23], the fluxes $F_R = F(U_R)$ and $F_L = F(U_L)$ are computed using the reconstructed solution vectors U_R and U_L on the right- and left-hand sides of the cell face respectively. The set of eigenvalues of the governing

equations can be obtained from the matrix A, where $A = \partial F/\partial U$ is evaluated using a symmetric average between U_R and U_L. The eigenvalues of the system matrix are given in Reference [1]. In the above equations, Δt is chosen as the local pseudo-time step, which is determined by the largest eigenvalue of the system of governing equations for each grid cell.

As usual, some two-phase flow phenomena are in the incompressible regime in which the particle and interfacial pressure may equal the gas pressure. This could leave an ill-posed mathematical model, which may require large numerical viscosity effects to achieve numerical stability. In order to avoid an ill-posed, two-fluid model, Saurel and Abgrall [1] considered both phases as compressible, which enables the system of equations to be well posed in terms of building artificial equations of state to model the flow of particulate phase. However, when the particulate phase is considered compressible, convergence difficulties may be encountered in the calculations while the particle phase is in the low Mach number limit. Therefore, we suggest that the AUSMD [20] is reformulated by the sound speed rescaled technique by Edwards and Liou [22] to operate effectively for the low-Mach number flow problems. The description of the AUSMD and the related rescaled scheme for the discretization of volume fraction equations and the convective flux of the dense and dilute phases are given in the following section, namely

3.1. Numerical flux

Dense phase

The flux formulas of the AUSMD have been demonstrated to be robust and low dissipated for the low-speed gas flow problem in Reference [21]. Here it is illustrated along one of the co-ordinate lines as the followings:

Let us begin by defining a common (interface) speed of sound

$$a_{1/2} = \frac{1}{2}(a_R + a_L) \tag{23}$$

where subscripts 'L' and 'R' denote the 'left' and 'right' states with respect to the interface.

In order to operate effectively in the low Mach number flow field, the AUSMD is reformulated by the rescaled technique as

$$\bar{a} = f_{1/2} a_{1/2} \tag{24}$$

where

$$f_{1/2} = \frac{\sqrt{(1 - M_\infty^2)^2 M_{1/2}^2 + 4M_\infty^2}}{(1 + M_\infty^2)} \tag{25}$$

the 'left' and 'right' Mach numbers are then redefined by the 'preconditioned' speed of sound as

$$M_L = \frac{u_L}{\bar{a}_{1/2}}; \qquad M_R = \frac{u_R}{\bar{a}_{1/2}} \tag{26}$$

However, the interface flux of the AUSMD scheme is still same as

$$F_{1/2} = \frac{1}{2}\bar{a}_{1/2}(\rho M)_{1/2}[\Phi_L + \Phi_R] - \frac{1}{2}|(\rho M)_{1/2}|\Delta_{1/2}\Phi + P_{1/2} \tag{27}$$

where $\Delta_{1/2}(\cdot) = (\cdot)_R - (\cdot)_L$, $\Phi = [\alpha, \alpha u, \alpha v, \alpha H, \alpha k, \alpha\varepsilon]$, and $P = [0, P, 0, 0, 0, 0]$, where the interface mass flux is also written as

$$(\rho M)_{1/2} = \rho_L M_L^+ + \rho_R M_R^- \tag{28}$$

Here (M_L^+, M_R^-) are defined as

$$M_L^+ = \alpha_L\left(\frac{(M+1)^2}{4} - \frac{M+|M|}{2}\right)_L + \frac{M_L + |M_L|}{2} \tag{29}$$

and

$$M_R^- = \alpha_R\left(-\frac{(M-1)^2}{4} - \frac{M-|M|}{2}\right)_R + \frac{M_R - |M_R|}{2} \tag{30}$$

where the parameter α is determined such that the numerical dissipation for the contact discontinuity vanishes and keeping the pressure equilibrium across material interface and can have several choices. In this paper, a weighting function based only on the ratio of pressure to density is defined as

$$\alpha_L = \frac{2(p/\rho)_L}{(p/\rho)_L + (P/\rho)_R}, \qquad \alpha_R = \frac{2(p/\rho)_R}{(p/\rho)_L + (p/\rho)_R} \tag{31}$$

to be a specific condition for pressure being continuous across the contact discontinuities.

The numerical flux AUSMD associated with the above velocity splitting automatically results in a vanished mass flux

$$(\rho M)_{1/2} = 0 \tag{32}$$

thus avoiding excessive numerical dissipation while solving a stationary contact discontinuity, where $M_j = M_{j+1} = 0$ and $p_j = p_{j+1}$. Also, the common speed of sound in the velocity and pressure splitting enables numerical fluxes to reproduce the exact Riemann solution of the contact discontinuities. This is the reason why the current numerical scheme allows exact capturing of stationary discontinuities in the single component problem [20]. Here we investigate its accuracy in solving multi-phase flow problems. We get the following

Volume Fraction Equation

Based on the upwinding interpolation delivered by AUSM scheme, the volume fraction equation (1a) can be evaluated by

$$\alpha_i^{n+1} = u_i^n - \lambda[h_{i+1/2}^n - h_{i-1/2}^n] \tag{33}$$

$$h_{i+1/2} = \frac{1}{2}[a_{\mathrm{I},i+1/2} M_{i+1/2}(\alpha_\mathrm{L} + \alpha_\mathrm{R}) - a_{\mathrm{I},i+1/2}|M_{i+1/2}|(\alpha_\mathrm{R} - \alpha_\mathrm{L})] \tag{34}$$

where $a_{\mathrm{I},i+1/2}$ is the sound of speed at the cell interface and $M_{i+1/2}$ is the mixture Mach number for each phase at the cell interface. $\lambda = \Delta t/\Delta x$, α_L and α_R can be obtained by a third-order accurate MUSCL extrapolated with a minmod limiter.

Dilute Particulate Phase

For the dilute particle phase, the volume fraction of the particulate phase is assumed very small as $\alpha_\mathrm{p} \ll 1$. Thus, the volume fraction of the gas phase is regarded as $\alpha_\mathrm{g} \approx 1$. In this study, the mass of particles per unit volume of mixture, $\rho_\mathrm{p} = \alpha_\mathrm{p}\rho_\mathrm{s}$, where ρ_s is the particle material density. In addition, the particulate pressure term for the dilute two-phase flow case is neglected. The system equations for dilute particulate flows can be simplified as the works of Tu [6,7]. Without the pressure term, the velocity splitting of the AUSMD and its interface numerical flux are simply modified as

$$F_{1/2} = u_{\mathrm{p},1/2}^{+}\Phi_\mathrm{L} + u_{\mathrm{p},1/2}^{-}\Phi_\mathrm{R} = \frac{1}{2}a_{\mathrm{p},1/2}M_{\mathrm{p},1/2}(\Phi_\mathrm{L} - \Phi_\mathrm{R}) - \frac{1}{2}a_{\mathrm{p},1/2}|M_{\mathrm{p},1/2}|(\Phi_\mathrm{R} - \Phi_\mathrm{L}) \tag{35}$$

where $M_{\mathrm{p},1/2}$ is the interface particle velocity defined as

$$(M_\mathrm{p})_{1/2} = M_{\mathrm{p,L}}^{+} + M_{\mathrm{p,R}}^{-} \tag{36}$$

with

$$M_\mathrm{p}^{\pm} = \frac{1}{2}(M_\mathrm{p} \pm |M_\mathrm{p}|)$$

and $\Phi = [\rho_\mathrm{p}, \rho_\mathrm{p}u_\mathrm{p}, \rho_\mathrm{p}v_\mathrm{p}, e_\mathrm{p}]$.

4. BOUNDARY CONDITIONS

At the inlet or exit of the computational domain, the subsonic characteristic boundary conditions are specified for ρ, u, P, e, k, ε for both phases. The no-slip boundary condition is used for the velocities on the solid surface. The specification of k at the closest-wall nodes is accomplished by assuming local equilibrium of the flow in the wall region. Also, ε at the nearest-wall nodes are determined by the turbulence length scale and vary linearly with

distance from the wall [25]. For the particular phase, the slip flow condition is assumed for the solid boundary conditions as

$$(u_{\mathrm{p}})_{\mathrm{wall}} = \tau_m \left[\frac{2}{3}(k + k_{\mathrm{p}}) - 2k \left(\frac{T_{\mathrm{L}}}{\tau_m + T_{\mathrm{L}}} \right) \right]^{1/2} \left(\frac{\partial u_{\mathrm{p}}}{\partial n} \right)_{\mathrm{wall}} \tag{37}$$

where

$$k_{\mathrm{p}} \cong k \frac{T_{\mathrm{L}}}{\tau_m + T_{\mathrm{L}}} \tag{38}$$

with

$$\tau_m = \frac{\rho_{\mathrm{p}} d_{\mathrm{p}}^2}{18 \mu^{\mathrm{eff}}} \tag{39}$$

and

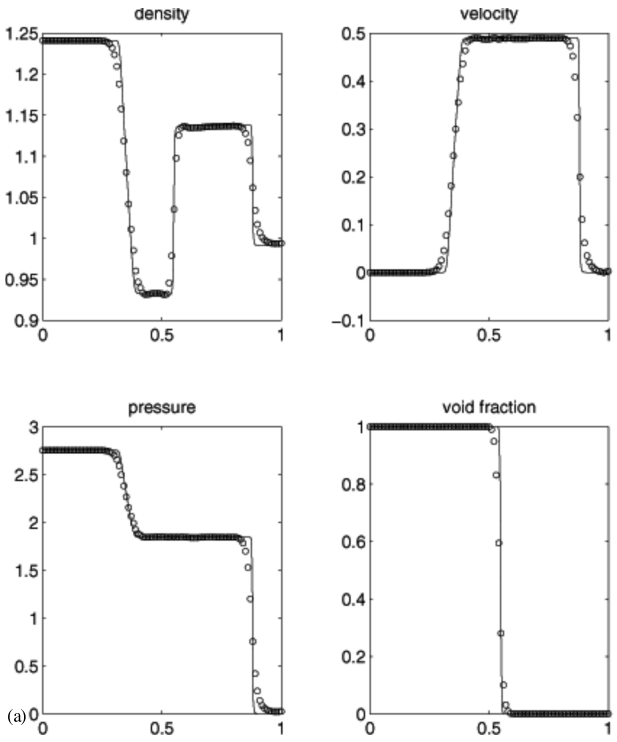

Figure 1. Numerical solutions of a two-phase gas–liquid shock tube based on (a) 100 and (b) 200 cells.

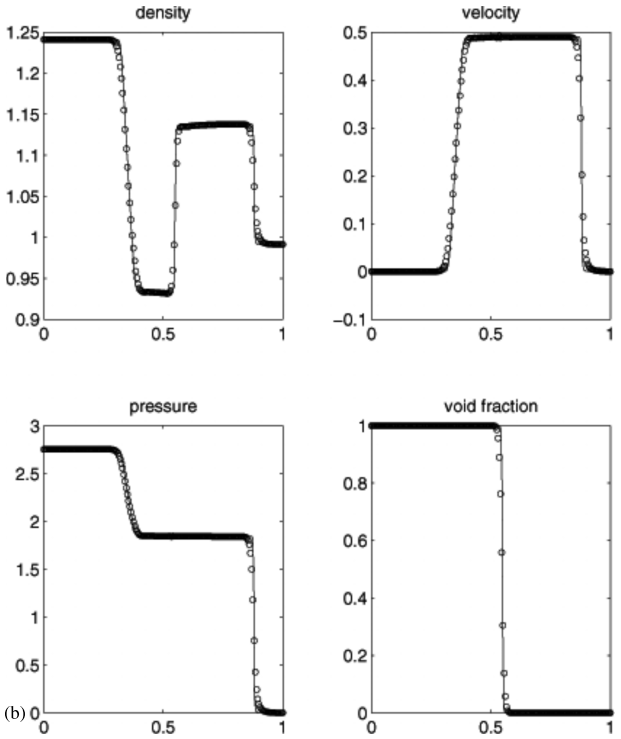

Figure 1 (*Continued*)

$$T_{\mathrm{L}} = C_T \frac{k}{\varepsilon} \tag{40}$$

where $c_T = 0.41$.

5. RESULTS AND DISCUSSION

5.1. Air–liquid shock tube

Following the work of Shyue [17], a two-phase gas–liquid Sod's problem, involving gas and liquid phases separated by an interface, is solved. The numerical capability of the AUSMD scheme on the resolution of material interfaces is investigated. This is a simplification of the underwater explosion problem in a spherically symmetric geometry. We consider a shock tube filled on its left part with high-pressure gas and on its right part with low-pressure liquid, under different ratios of specific heat. Also, the stiffened gas equation of state is used to describe the liquid phase. This belongs to an interface problem that the solution of a Riemann

problem consists of a single contact discontinuity in gas dynamics [17]. Numerical solution is obtained by which the liquid flow is governed by a stiffened equation of state [1,17]

$$P = (\gamma - 1)\rho e - \gamma\pi \tag{41}$$

We have a stiffened gas and use two constant states as

$$\begin{pmatrix} \rho \\ u \\ p \\ \gamma \\ p_\infty \end{pmatrix}_{\mathrm{L}} = \begin{pmatrix} 1.241 \\ 0 \\ 2.753 \\ 1.4 \\ 0 \end{pmatrix} \quad \text{and} \quad \begin{pmatrix} \rho \\ u \\ p \\ \gamma \\ p_\infty \end{pmatrix}_{\mathrm{R}} = \begin{pmatrix} 0.991 \\ 0 \\ 3.056 \times 10^{-4} \\ 5.5 \\ 1.505 \end{pmatrix} \tag{42}$$

Here L is the state used for $x \in [0, 0.5)$ and R is the state used for $x \in [0.5, 1]$.

The solution is plotted at time 0.1. Mixture pressure, mixture density, velocities, and gas void fraction contain exact solutions, which are represented by solid lines in Figure 1(a) and (b). The computed solutions are performed on constant spacing meshes of 100 cells and 200 cells. The MUSCL extrapolation with a minmod limiter is utilized. A Courant–Friedrich–

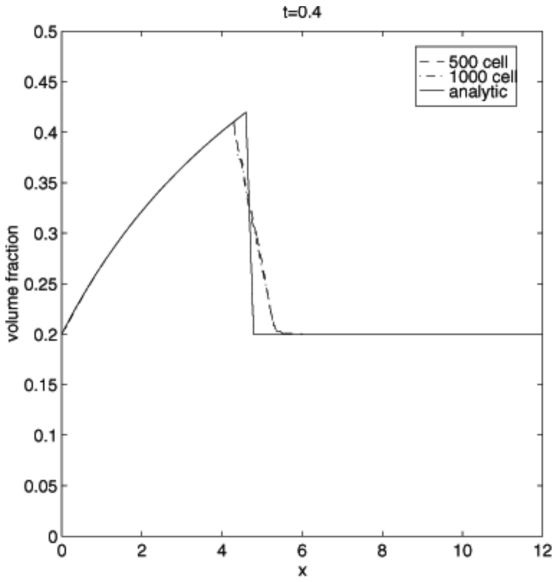

Figure 2. The volume fraction profile of the water faucet at $t = 0.4$.

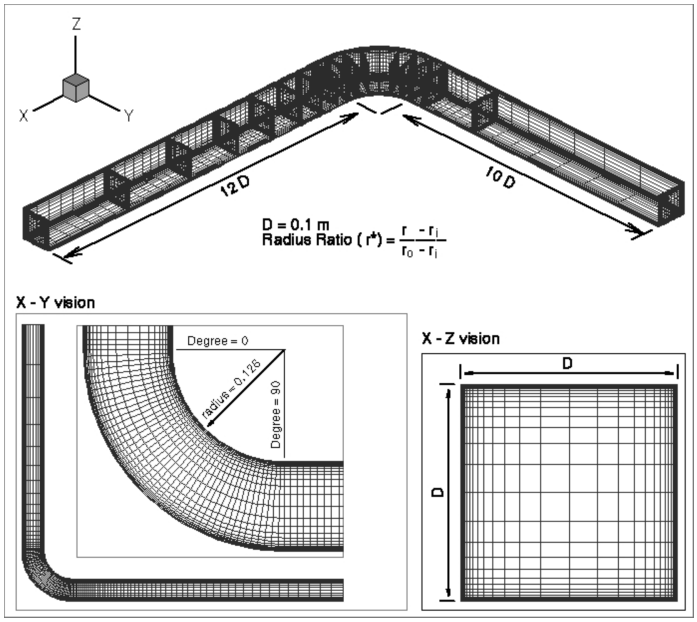

Figure 3. Computation domain of a three-dimensional 90° bend on $120 \times 31 \times 31$ grid (sketched from Tu and Fletcher [6]).

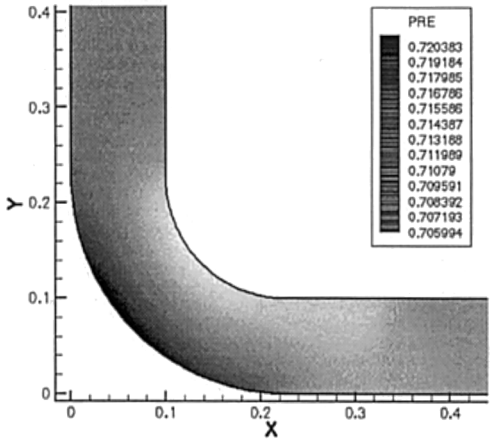

Figure 4. Gas flow pressure distribution of a 90° bend.

Lewy (CFL) number of 0.5 is chosen to keep numerical stability. The comparisons show that the agreement between exact solutions and computed results is satisfactory. Numerical oscillation around the contact discontinuity is removed regardless if the grid cell is coarse or fine. Also, the computed void fraction is shown to be non-oscillatory. It is noted that the AUSMD contains the mechanism exactly to capture of the contact discontinuity without excessive numerical dissipation, and keeps the pressure continuous across material interfaces based on a weighting function of the ratio of pressure to density. Besides the correct behaviors of shock waves, rarefaction and void fraction are also seen in the computed results.

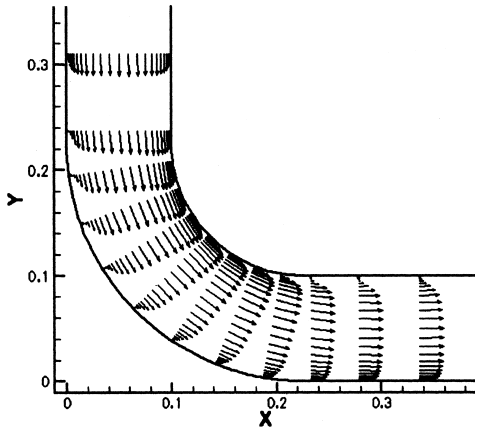

Figure 5. Gas velocity vector profile of a 90° bend.

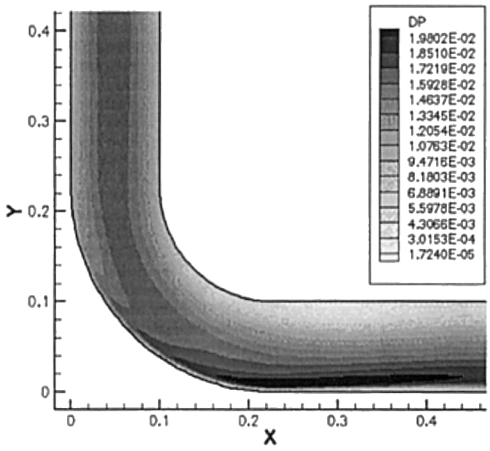

Figure 6. Particulate concentration plot of a 90° bend.

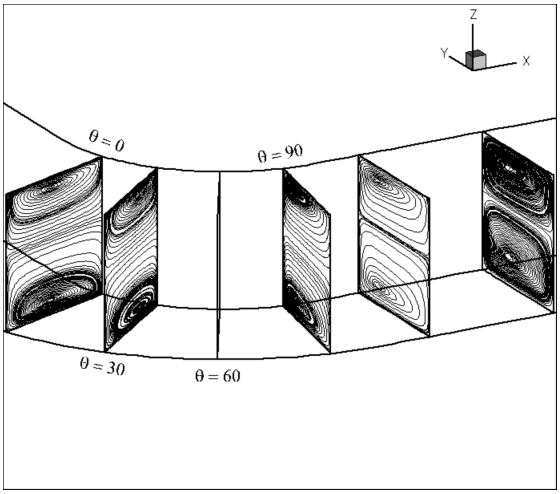

Figure 7. The streamtrace plot at cross-sections along the bend.

5.2. Water faucet

The water 'faucet' problem tested in Reference [24] consists of a liquid stream with a fixed inflow rate of water at a velocity of 10.0 m s^{-1}, a temperature of 50°C, and a liquid volume fraction of 0.8 entering a vertical tube 12 m in length and 1.0 m in diameter from the top. Due to the action of gravity, the water falls to form a stream of uniformly decreasing cross-section. The bottom of the tube is open to the ambient pressure. The objective of this problem is to test numerical viscosity and stability on the resolution of void propagation.

To perform the calculations, a liquid volume fraction of 0.8 and a vapor volume fraction of 0.2 with a temperature of 50°C, a pressure of 1.0E05 Pa are used for the initial conditions. Water convects with a uniform velocity of 10.0 m s^{-1} surrounded by stagnant vapor. The boundary conditions at the inlet to the top of the tube are constant fluid thermodynamic conditions and constant liquid inflow velocity. The liquid state is at 50°C and 1.0E05 Pa. The vapor boundary conditions is arbitrary since the inflow rate is zero. The velocity boundary conditions are 10.0 m s^{-1} for the liquid and 0.0 m s^{-1} for the vapor. The volume fraction for the liquid at the inlet is constant at 0.8. The only outflow boundary condition at the bottom of the tube is constant pressure at 1.0E05 Pa.

Mass effects, wall fraction, and interphase friction are not considered in this case. It is assumed that the liquid–vapor interface is uniform and the phasic pressure is same at each location. This transient problem has a particularly simple analytical solution [11] when pressure variation in the vapor phase is ignored. The computations are performed using a constant CFL number (0.5) on the cells of 500 and 1000 respectively. The MUSCL extrapolation with a minmod limiter is utilized. The computed volume fraction of vapor at a time of 0.4 s compared with the analytic solutions is shown in Figure 2. It is seen that both meshes, with 500 cells and 1000 cells, capture the discontinuity of the void fraction, but smear out the peak

value to some extent. However, to compare with the previous computations provided in Reference [11] for the same case, current results are satisfactory.

5.3. 90° Bend

In the final test case, dilute solid–gas turbulent flows passing through a 90° bend are investigated. A very dilute particle suspension in the radial, streamwise, and spanwise directions is assumed as in Kliafas and Holt(s experiment [28]. Their experimental data are chosen to validate the current work. A dilute particulate turbulence flow model based on the RNG theory proposed by Tu and Fletcher [6,7] is used here. The flow conditions used in the

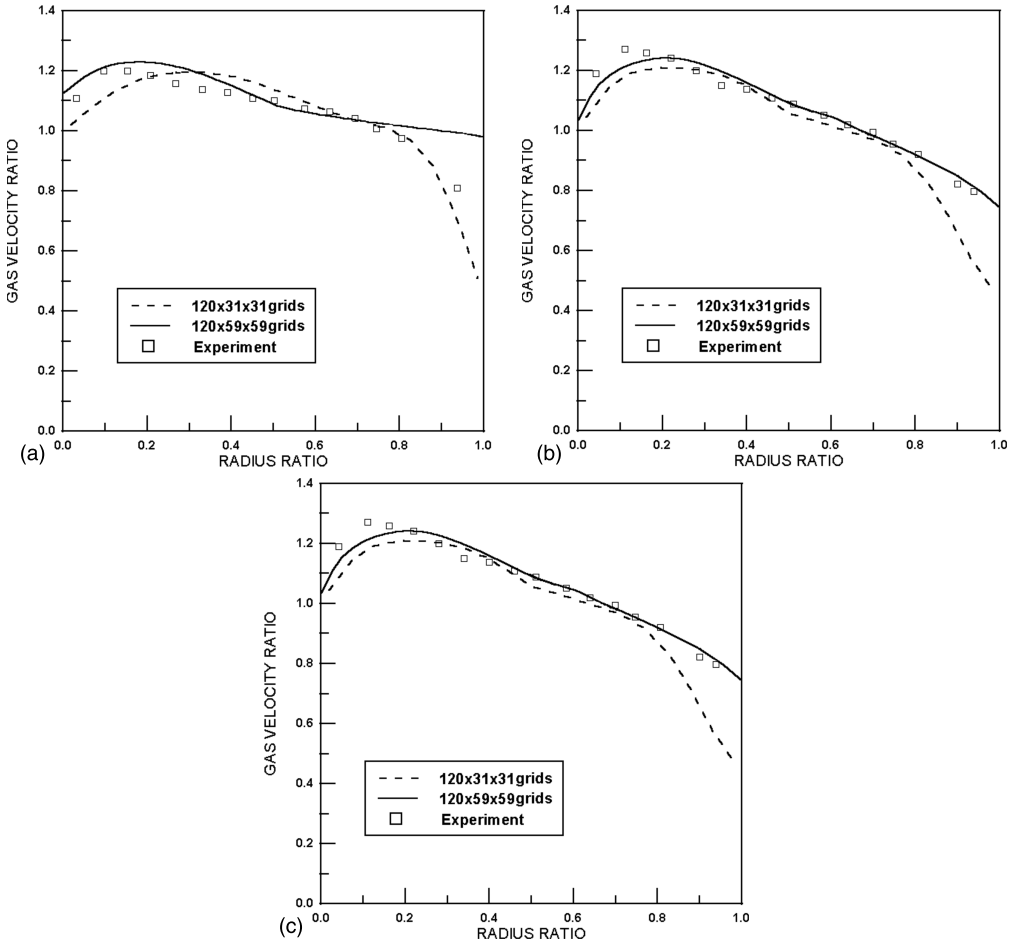

Figure 8. Gas phase velocity profile at (a) $\theta = 0°$, (b) $\theta = 15°$, and (c) $\theta = 30°$ station of the bend.

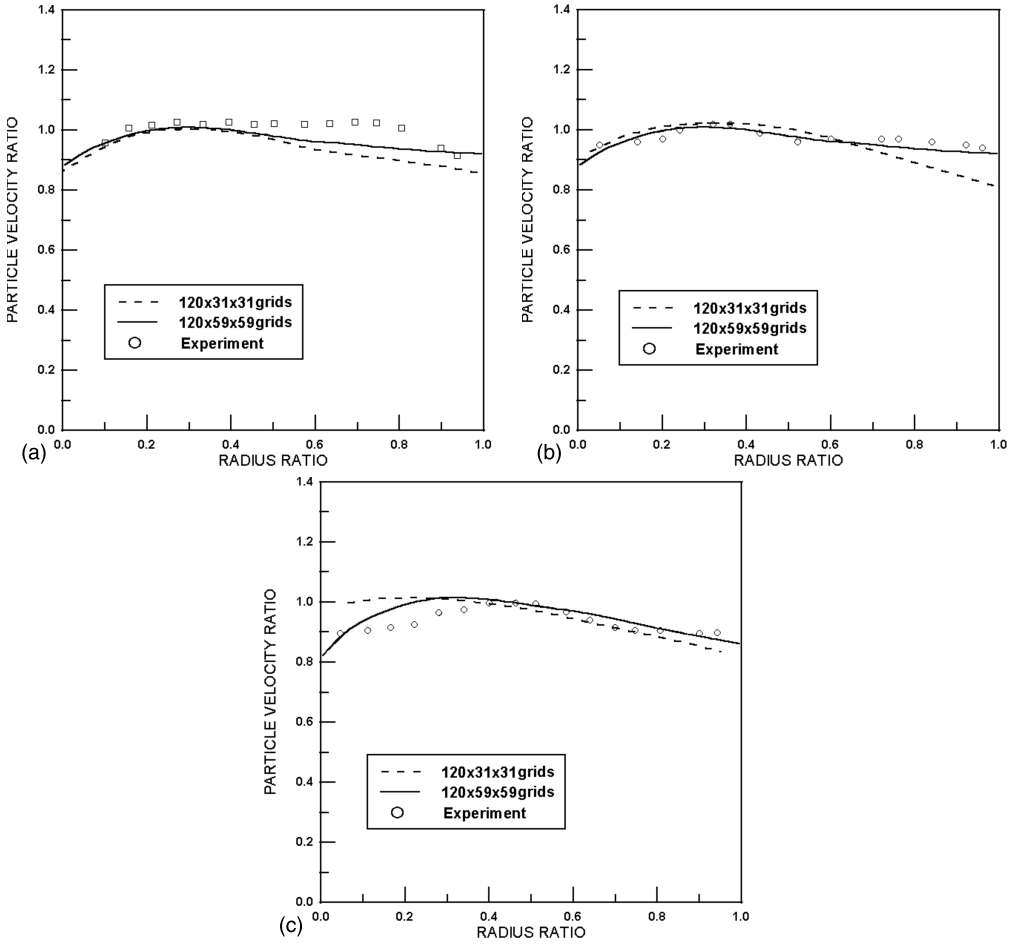

Figure 9. Particulate phase velocity profile at (a) $\theta = 0°$, (b) $\theta = 15°$, and (c) $\theta = 30°$ station of the bend.

computations [6] for the comparison with the experiment are $U_b = 52.19\ \mathrm{m\,s^{-1}}$, corresponding to the Reynolds number 3.47×10^5, the inlet turbulence intensity of the gas phase at 1 per cent, the particle diameter size 50 μm, the particle material density $\rho_s = 2990\ \mathrm{kg\,m^{-3}}$, the inlet particulate bulk density $\rho_p = 1.8 \times 10^{-4}\ \mathrm{kg\,m^{-3}}$. In this study, $120 \times 31 \times 31$ grids shown in Figure 3 are generated for the computations.

Figures 4 and 5 shows numerical predictions of gas flow through a 90° bend in terms of pressure contour and velocity vector distributions. The maximum values of gas velocity profiles are found to displace toward the inner wall, as a result of favorable streamwise pressure gradients present. It is also found that there is deceleration of the flow near the outer wall due to adverse pressure gradients near the inner wall. Figure 6 shows particulate

concentrations in the same plane. Here we can find that particles following the gas flow into the bend entrance and then, due to their own inertia, collide with the outer wall directly. Along the turning section of the bend, a much higher particle concentration appears near the outer wall than near the inner wall. It is also seen from Figure 6 that very few particles are found in the region near the inner wall of the bend. A particle-free region is simulated close to the inner wall. The thickness of this particle-free region gradually increases toward downstream. It can be noted that particle–wall collision is significant in the flow region near the outer wall. Only the outer wall is impacted by particles and the inner wall is generally free of erosion. This is consistent with the observation by Kliafas and Holt and the results computed by Tu and Fletcher. Figure 7 depicts the stream trace plot of the gas phase at transverse planes along the

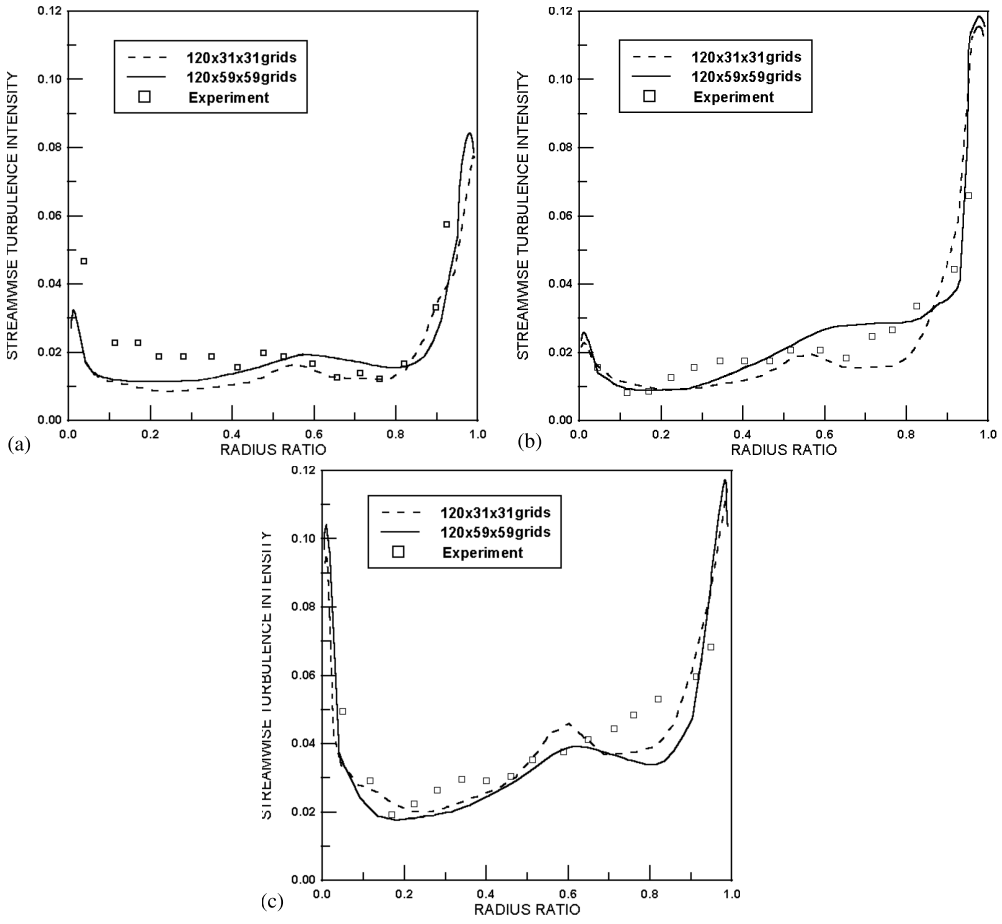

Figure 10. Streamwise turbulence intensity profile at (a) $\theta = 0°$, (b) $\theta = 15°$, and (c) $\theta = 30°$ station of the bend.

bend. It is shown that a pair of flow vortex appears at each cross-section of the turning tube. A strong secondary effect is captured in the calculations.

Next, mean streamwise gas velocity profiles at the $\theta = 0°$, 15°, and 30° stations are computed and compared with measured data as shown in Figure 8(a)–(c). In Figure 9(a)–(c), the particle velocity profile distributions compared with validated data are demonstrated. The results computed on coarse and fine grids are also shown. From Figures 8 and 9, it is observed that the large negative slip velocity between the gas and particulate flow appears near the outer wall. The maximum values of gas velocity profiles are displaced toward the inner wall, as a result of favorable streamwise pressure gradients present there. However, the gas pressure does not affect the distributions of particulate velocity. A relatively uniform particle velocity profile at all stations is obtained. It can be seen from these figures that the fine grid has yielded almost identical solutions with Kliafas and Holt(s measurements.

The predictions of streamwise turbulence intensity for location $\theta = 0°$, 15°, and 30° by an RNG-based k–ε turbulence model, compared with the measurements, are presented in Figure 10(a)–(c). The high turbulence intensity near the two side walls is observed. It is shown that the predictions on the fine grid agree with experimental data very well. The current RNG-based k–ε turbulence model demonstrates very good accuracy.

6. CONCLUSIONS

In this study a seven-equation compressible two-fluid model containing a non-conservative evolution equation of volume fraction and six conservation equations is expressed in the hyperbolic form. The AUSMD is modified to discretize the volume fraction equation and the convection equations for the dense and dilute phases. Test cases involving an air–water shock tube, water faucet, and dilute particulate turbulent flows through a 90° bend are used to verify the computations. It is shown that the AUSMD contains the mechanism to correctly capture the contact discontinuity and interfaces between phases without excessive numerical dissipation. Besides, the RNG-based k–ε model containing particle–wall collision terms achieve accurate prediction of wall quantities for both gas and particle phases. Numerical results reveal that the AUSMD has demonstrated simplicity and accuracy in solving the compressible two-fluid model and achieved successful applications to dilute particulate turbulence flow problems.

ACKNOWLEDGMENTS

The author wishes to acknowledge the support sponsored by the National Science Council of Taiwan under Contract NSC-89-TPC-7-216-002. The author also acknowledges fruitful discussions on the AUSM with Dr M. S. Liou from NASA John H. Glenn Research Center, USA.

REFERENCES

1. Saurel R, Abgrall R. A multiphase Godunov method for compressible multifluid and multiphase flows. *Journal of Computational Physics* 1999; **150**: 425–467.

2. Saurel R, Forestie A, Veyret D, Loraud JC. A finite-volume scheme for two-phase compressible flows. *International Journal for Numerical Methods in Fluids* 1994; **18**: 803–819.
3. Rizk MA, Elghobahsi SE. A two-equation turbulence model for dispersed dilute confined two-phase flow. *International Journal of Multiphase Flow* 1989; **15**: 119–133.
4. Adeniji-Fashola A, Chen CP. Modeling of confined turbulent fluid-particle flows using Eulerian and Lagrangian schemes. *International Journal of Heat and Mass Transfer* 1990; **33**: 691–701.
5. Issa RT, Oliverira PJ. Numerical prediction of phase separation in two-phase flow through T-junctions. *Computers and Fluids* 1994; **23**: 347–372.
6. Tu JY, Fletcher CAJ. Numerical computation of turbulent gas–solid particle flow in 90° bend. *AIChE Journal* 1994; **41**: 2187–2196.
7. Tu JY, Fletcher CAJ, Behnia M. Numerical modelling of three-dimensional fly-ash flow in power utility boilers. *International Journal for Numerical Methods in Fluids* 1997; **24**: 787–807.
8. Raviart PA, Sainsaulieu L. A non conservative hyperbolic system modeling spray dynamics. Part I: solution of Riemann problem. *Mathematical Models and Methods in Applied Sciences* 1995; **5**: 297–333.
9. Sainsaulieu L. Finite-volume approximation of two phase-fluid flows based on an approximate Roe-type Riemann solver. *Journal of Computational Physics* 1995; **121**: 1–28.
10. Tonmi I, Kumbaro A. An approximate linearized Riemann solver for two-fluid model. *Journal of Computational Physics* 1996; **124**: 286–300.
11. Coquel G, Amine KE, Godlewski E, Perthame B, Rascle P. A numerical method using upwind schemes for the resolution of two-phase flows. *Journal of Computational Physics* 1997; **136**: 272–288.
12. Abgrall R. Generalization of Roe's Riemann solver to mixtures of perfect gas. *La Recherche Aérospatiale* 1988; **6**: 31–43.
13. Karni S. Multi-component flow calculations by a consistent primitive algorithm. *Journal of Computational Physics* 1994; **112**: 31–43.
14. Jenny P, Mueller B, Thomann H. Correction of conservative Euler solvers for gas mixtures. *Journal of Computational Physics* 1997; **132**: 91.
15. Abgrall R. How to prevent pressure oscillations in multi-component flow calculations: a quasi conservative approach. *Journal of Computational Physics* 1996; **125**: 150–160.
16. Karni S. Hybrid multifluid algorithms. *SIAM Journal of Scientific Computing* 1996; **17**: 1019.
17. Shyue KM. An efficient shock-capturing algorithm for compressible multi-component problems. *Journal of Computational Physics* 1998; **142**: 208–242.
18. LeVeque RJ. Wave propagation algorithm for multi-dimensional hyperbolic systems. *Journal of Computational Physics* 1997; **131**: 327.
19. YY Niu. Simple conservative flux splitting for multi-component flow calculations. *Numerical Heat Transfer* 2000; part B, No. 2, **38**: 203–222.
20. Liou MS, Wada Y. A quest towards ultimate numerical flux schemes. In *Computational Fluid Dynamics Review 1995*, Hafez M, Oshima K (eds). Wiley: New York, 1995; 251–278.
21. Niu YY, Liou MS. Numerical simulation of dynamic stall using upwind schemes and dual time stepping. *AIAA Journal* 1999; **36**: 1386–1392.
22. Edwards JR, Liou MS. Low-diffusion of flux splitting methods for flows at all speeds. *AIAA Journal* 1998; **36**: 1610–1617.
23. van Leer B. Towards the ultimate conservative difference, V: a second order sequel to Godunov's method. *Journal of Computational Physics* 1979; **32**: 179–186.
24. Ransom VH. Numerical benchmark tests. In *Multiphase Science and Technology*, vol. 3, Hewitt GF, Delhay JM, Zuber N (eds). Hemisphere Publishing: Washington, DC, 1993; 465–467.
25. Pourahmadi F, Humphrey JAC. Modeling solid–fluid turbulent flows with application to predicting erosive wear. *Physicochemical Hydrodynamics* 1983; **4**: 191–219.
26. Kliafas Y, Holt M. LDV measurements of a turbulent air–solid two-phase flow in a 90-degree bend. *Experimental Fluids* 1987; **5**: 73.
27. Strang G. On the construction and comparison of difference schemes. *SIAM Journal of Numerical Analysis* 1968; **5**: 506–517.
28. Yakhot V, Orszag S. A renormalization group analysis of turbulence. *Journal of Scientific Computing* 1986; **1**: 3–51.

